AGU PUBLICATIONS

Water Resources Research

RESEARCH ARTICLE
10.1002/2014WR015381

Lateral subsurface stormflow and solute transport in a forested hillslope: A combined measurement and modeling approach

Hanne Laine-Kaulio[1], Soile Backnäs[2], Tuomo Karvonen[3], Harri Koivusalo[1], and Jeffrey J. McDonnell[4,5]

[1]Water and Environmental Engineering, Aalto University School of Engineering, Espoo, Finland, [2]Geological Survey of Finland, Kuopio, Finland, [3]Waterhope, Helsinki, Finland, [4]Global Institute for Water Security, University of Saskatchewan, Saskatoon, Saskatchewan, Canada, [5]School of Geosciences, University of Aberdeen, Aberdeen, UK

Key Points:
- Preferential flow mechanisms control lateral subsurface stormflow in forest till
- A two pore domain approach is needed to model the coupled flow and transport
- Tracer data facilitate the model parameterization and testing

Correspondence to:
H. Laine-Kaulio,
hanne.laine@aalto.fi

Citation:
Laine-Kaulio, H., S. Backnäs, T. Karvonen, H. Koivusalo, and J. J. McDonnell (2014), Lateral subsurface stormflow and solute transport in a forested hillslope: A combined measurement and modeling approach, *Water Resour. Res.*, *50*, 8159–8178, doi:10.1002/2014WR015381.

Received 29 JAN 2014
Accepted 22 SEP 2014
Accepted article online 26 SEP 2014
Published online 21 OCT 2014

Abstract Preferential flow dominates water movement and solute transport in boreal forest hillslopes. However, only a few model applications to date have accounted for preferential flow at forest sites. Here we present a parallel and coupled simulation of flow and transport processes in the preferential flow domain and soil matrix of a forested hillslope section in Kangaslampi, Finland, using a new, three-dimensional, physically based dual-permeability model. Our aim is to simulate lateral subsurface stormflow and solute transport at the slope during a chloride tracer experiment, and to investigate the role of preferential flow in the tracer transport. The model was able to mimic the observed tracer transport during tracer irrigation, but overestimated the dilution velocity of the tracer plume in the highly conductive soil horizons near the soil surface after changing the irrigation to tracer-free water. According to the model, 140 times more chloride was transported downslope in the preferential flow domain than in the soil matrix during the tracer irrigation. The simulations showed, together with reference simulations with a traditional one pore domain model, that a two pore domain approach was required to simulate the observed flow and transport event. The event was characterized by the transmissivity feedback phenomenon and controlled by preferential flow mechanisms, in particular by lateral by-pass flow. According to our results, accounting for the slow-flow and fast-flow domains of soil, as well as the water and solute exchange between the domains, is essential for a successful simulation of flow and solute transport in preferential flow dominated hillslopes.

1. Introduction

Preferential flow paths influence water flow and solute transport in forested hillslopes [e.g., *Uchida et al*., 2005]. These flow paths are networks of large pores (i.e., macropores), soil pipes, and other void spaces in soil that are typically formed by soil fauna, live roots, decayed root channels, and tree stems, as well as by erosive actions and freezing-thawing phenomena [*Aubertin*, 1971; *Beven and Germann*, 1982, 2013; *Koch et al*., 2013]. Preferential flow controls the vertical infiltration of water and solutes into soil, as well as the lateral movement of water and solutes along hillslopes toward streams and catchment outlets [e.g., *Klaus et al*., 2013]. Preferential flow may either accelerate or delay the movement of dissolved matter, depending upon the prestorm spatial distribution of the matter compared to the locations of the preferential flow paths [*Allaire et al*., 2009].

Runoff from forested hillslopes to streams typically takes place via subsurface routes [*Bachmair and Weiler*, 2011]. Flow through preferential pathways enhances the infiltration of water into soil, it can displace older water stored in the soil matrix deeper into the soil or move it toward the streams [e.g., *Mosley*, 1979; *Pearce et al*., 1986; *McDonnell*, 1990], and generate fast lateral subsurface stormflow along hillslopes, for instance, due to the transmissivity feedback phenomenon [e.g., *Bishop*, 1991]. In till mantled forested hillslopes, the fraction of event water may be greater for wet antecedent moisture conditions, and event water may even dominate the runoff signature during large storm events [e.g., *Lepistö et al*., 1994]. The interactions between the soil matrix and hillslope preferential flow systems influence the ability of forest soil to retain, release, and transport nutrients under different soil moisture conditions [*Backnäs et al*., 2012].

Despite the increasing knowledge on runoff from forested hillslopes, hillslope-scale lateral flow, and solute transport are still poorly measured and modeled. Traditional models, based on the Darcy-Richards approach [*Richards*, 1931], describe the soil pore space as one pore domain. They often fail in reproducing the real

subsurface flow and transport events because only preferred fractions of the total soil pore space control the flow and transport [e.g., *Espeby*, 1989; *Jansson et al*., 2005; *James et al*., 2010]. For instance, at the Panola Mountain Experimental Hillslope in Georgia, *Hopp and McDonnell* [2009] and *James et al*. [2010] used traditional Dacry-Richards models that were only able to represent half of the measured hillslope discharge; the other half was lateral pipe flow that could not be simulated by the model if internal pore pressure dynamics were used as an evaluation criteria. Many have argued that two pore domains are needed in computational models to describe subsurface stormflow in forest soils [e.g., *Weiler and McDonnell*, 2007].

A number of two pore domain models have been developed to divide the soil pore space into slow-flow and fast-flow regimes [e.g., *Gerke and van Genuchten*, 1993a, 1993b; *Šimůnek et al*., 1999, 2012; *Vogel et al*., 2000; *Jansson and Karlsberg*, 2001; *Larsbo and Jarvis*, 2003; *Ray et al*., 2004; *Gerke et al*., 2007; *Laine-Kaulio*, 2011; *Warsta*, 2011; *Dušek et al*., 2012]. The models represent different combinations of governing equations for flow in the preferential flow domain (e.g., Richards' equation or kinematic wave equation), mathematical descriptions of the exchange of water, and solutes between the pore domains (e.g., dependency on the moisture status of the preferential flow domain or on the moisture status of both pore domains), flow dimensions (i.e., 1-D, 2-D, or 3-D flow), model type (dual-porosity or dual-permeability approach), and numerical solution methods and algorithms used (e.g., control difference, finite volume, or control volume method) [e.g., *Gerke*, 2006].

Almost all available applications of the two pore domain models to date are for agricultural sites [e.g., *Gärdenäs et al*., 2006; *Köhne et al*., 2006; *Vogel et al*., 2007; *Dušek et al*., 2010; *Warsta et al*., 2013]. The few studies that have applied two pore domain models in forest sites include early work by *Espeby* [1989] for a small forested catchment in Sweden using the SOIL model (developed originally by *Jansson and Halldin* [1979]) and more recent work by *Jansson et al*. [2005] in the same site with a new version of the SOIL model, COUP [*Jansson and Karlsberg*, 2001]. These 1-D models use a simple by-pass routine for preferential flow. More detailed, physically based, 1-D, dual-permeability simulations have recently been conducted in the Czech Republic for discharge estimations from a forested hillside [e.g., *Dohnal et al*., 2012; *Dušek et al*., 2012]. While more complex 3-D approaches have been conducted for forested hillslopes in, e.g., Georgia, USA [e.g., *Hopp and McDonnell*, 2009; *James et al*., 2010], and Oregon, USA [*Ebel et al*., 2008], none have yet incorporated two pore domains for 3-D simulations of subsurface flow and solute transport in preferential flow dominated hillslopes.

Assessment of the structural adequacy of two pore domain models for forested hillslopes is restricted by the limited data availability for model parameterization, calibration, and validation [e.g., *Arora et al*., 2012]. Means to restrict the number of calibrated parameter values improves the assessment of the structural competence of a model. In addition, manipulation experiments producing data on solute concentrations can provide powerful means to test model structures by isolating individual flow mechanisms [*Kirchner*, 2006]. While *Iorgulescu et al*. [2005] and *Vaché and McDonnell* [2006] have shown the importance of natural isotopic tracer data for streamflow generation simulations, high-frequency chemical data on runoff generation are rare and have not been widely used for model evaluation [*Kirchner et al*., 2004; *Kirchner*, 2006]. New measurements, as well as advances in using them to reduce model and parameter uncertainty, are crucial for the development of hydrological models [*McDonnell and Tanaka*, 2001; *McDonnell and Beven*, 2014].

Here we apply a new, 3-D, physically based dual-permeability model to a forested hillslope section in Kangaslampi, Eastern Finland. Our objective is to simulate lateral subsurface stormflow and solute transport in the slope during a chloride tracer experiment, to investigate the role of preferential flow in the flow and transport event, and to describe and quantify with the model the lateral tracer transport along the slope. Our hypothesis is that a two pore domain approach is required for simulating the observed event. The use of our own source code makes it possible to modify the model and investigate the water and solute fluxes in and between the pore domains.

2. Material and Methods

2.1. Study Site

The Kangaslampi experimental hillslope is located in Eastern Finland (Figure 1a). It belongs to the middle boreal forest zone and is classified as Vaccinium-Myrtillus type according to the Finnish forest type classification [*Cajander*, 1949; *Mikola*, 1982]. The long-term (1971–2000) mean annual air temperature is +1.9°C

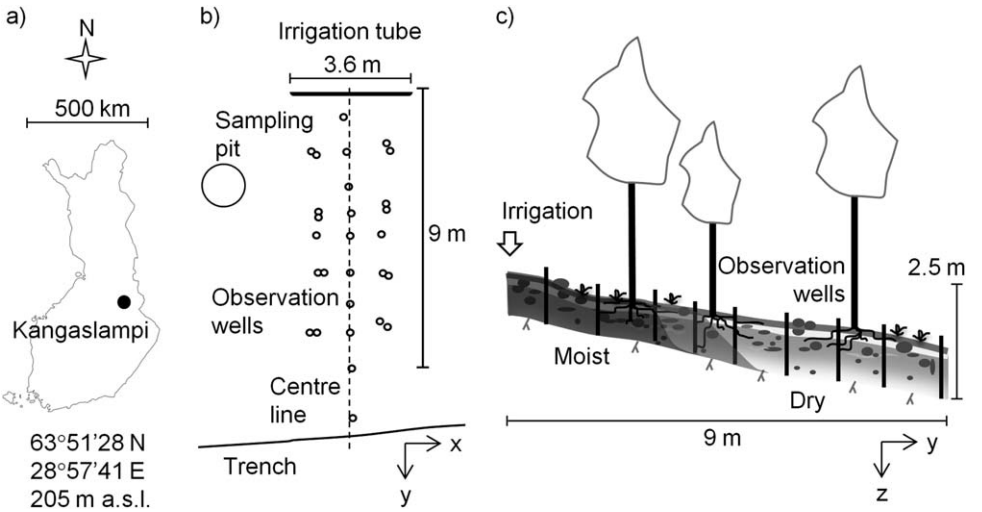

Figure 1. (a) Location of Kangaslampi in Finland, (b) map of the tracer experiment site, and (c) cross profile of the experimental hillslope section at the initial state of the experiment, following the centerline of the observation well field from the irrigation tube toward the trench.

and the mean annual precipitation is 564 mm with approximately 200 mm in the form of snow [*Piirainen et al*., 2007]. About half of the annual precipitation generates runoff, and the main yearly runoff event is induced by spring snowmelt. Topography is characterized by gently sloping hills that are surrounded by riparian areas, ponds, and small lakes.

The present study concentrated on a 15 m long section in the midslope area of the hillslope. Within this section, the mean slope was about 15% and the thickness of the mineral soil profile above bedrock was 69–116 cm. The soil type was haplic podzol with sandy till as the parent material [*Food and Agriculture Organization* (*FAO*), 1988], representing the most common soils in Finland. The podzol profile consisted of eluvial (E), illuvial (B), transitional (BC), and subsoil (C) horizons (Table 1), and the forest floor consisted of a 10 cm thick organic litter and mor humus layer (O). The B-horizon was partially cemented due to the formation of Ortstein by illuviated sesquioxides and organic matter. The bedrock was formed of gneiss granite and granodiorite and it was nearly impervious with minor fractures.

The field layer vegetation consisted of dwarf shrubs (*Vaccinium vitisidaea* L., *V. myrtillus* L., and *Empetrum nigrum*), and feather mosses (*Pleurozium schreberi*) dominated the bottom layer. The mixed, coniferous forest was approximately 70 years old, composing of Norway spruce (*Picea abies* Karsten, 55%), Scots pine (*Pinus sylvestris* L., 28%), and white birch (*Betula pubescens* Ehrh., 17%). The mean tree height was 20 m and the mean volume 273 m^3 ha^{-1}. Prior to the tracer experiment (section 2.2), the mineral soil column had not been treated or disturbed by forestry practices. The tree stand had been regularly thinned during the past but had no detectable impact on the soil.

2.2. Chloride Tracer Experiment

Data describing lateral subsurface stormflow and solute transport were compiled from a chloride tracer experiment that was conducted for applying a dual-permeability model to a forest site [*Laine-Kaulio*, 2011].

Table 1. Soil Physical Properties: Mean Value (Measured Range, Sample Size)[a,b,c]

Soil Horizon	Thickness (cm)	Parent Material, Texture	Stone Content (m^3 m^{-3})	Pore Volume (m^3 m^{-3})	Pore Volume Excl. Stones (m^3 m^{-3})
E	9 (5–14, 20)	ST (Si-G, 4)	0.34 (0.20–0.48, 10)	0.49 (0.40–0.61, 11)	0.32 (0.21–0.49)
B	14 (8–20, 20)	ST (S-G, 5)	0.30 (0.18–0.42, 10)	0.47 (0.30–0.57, 11)	0.33 (0.17–0.47)
BC	17 (8–30, 20)	ST (S-G, 5)	0.17 (0.10–0.24, 10)	0.40 (0.37–0.42, 9)	0.33 (0.28–0.38)
C	40 (28–52, 20)	ST (S, 5)	0.09 (0.05–0.12, 10)	0.34 (0.29–0.39, 6)	0.31 (0.26–0.37)

[a]For soil texture: G = gravelly, S = sandy, Si = silty, T = till.
[b]Pore volumes apply to soil cores, height 1.5–7.0 cm, diameter 3.8–5.4 cm.
[c]Variation of pore volume excl. stones derived from variations of stone content and pore volume data.

Table 2. Degree of Saturation [$m^3\ m^{-3}$] at the Beginning of Tracer Irrigation Within the Moist and Dry Parts of the Experimental Hillslope Section (Figure 1c)

Soil Horizon	Moist Part	Dry Part
E	0.64 (0.50–0.78)	0.29 (0.25–0.33)
B	0.79 (0.70–0.88)	0.42 (0.38–0.45)
BC	0.79 (0.67–0.91)	0.30 (0.27–0.33)
C	0.90 (0.84–0.96)	0.36 (0.33–0.39)

In the experiment, a perforated irrigation tube, connected to water tanks, was placed at the upslope edge of the experimental hillslope section that was instrumented with observation wells (Figure 1b). The slope was first irrigated with tracer-free water through the tube to create initial moisture conditions for the tracer experiment, where the upper part of the hillslope section was wet and the lower part was dry (Figure 1c). This was to investigate the lateral migration of the tracer plume in different antecedent soil moisture conditions.

The initial irrigation period was started 21 h before the tracer experiment and lasted for 2 h; the irrigated water volume was about 1.4 m^3. Before the initial irrigation, the soil at the hillslope was rather dry (degree of saturation 25–45%). During the irrigation, the soil saturated up to the E-horizon at a length of about 3 m downslope from the irrigation tube (Figure 1c). After the initial irrigation was stopped, the water table fell, and when the tracer irrigation was started the next day, no water table was observed above the bedrock. The measured degrees of saturation at the beginning of the tracer experiment are presented in Table 2. Between the moist and dry parts of the experimental hillslope section (Table 2 and Figure 1c), the degree of saturation was estimated to drop linearly.

In the tracer experiment on 6 September 2005, a volume of approximately 0.8 m^3 of 698 mg L^{-1} chloride solution was applied to the soil during 1 h 20 min (11:40–13:00) through the perforated tube (Figure 1b). The 698 mg L^{-1} concentration was about 32-fold compared to the natural chloride concentration measured in the soil water (i.e., 22 mg L^{-1}). During the following 2 h 10 min (13:00–15:10), the irrigation was continued with 1.3 m^3 of tracer-free water. However, the last 0.5 m^3 of the irrigation water contained small amounts of tracer (78 mg L^{-1}) because the last tank used for irrigation was used earlier for storing tracer solution and it contained remains of the tracer. The area where the irrigation spread under the irrigation tube was about 2 m^2. Thus, the average infiltration to soil during the irrigation was 295 mm h^{-1}. If the irrigated water volume is divided by the whole area of about 50 m^2 where a water table was formed in soil above the bedrock during the experiment, the irrigation corresponded to a rainfall event of 41 mm.

During the irrigation and for 3 h 40 min afterward, water table and chloride concentration were recorded in the observation wells (outside diameter 40 mm, inside diameter 31 mm). The wells were screened, and the screen holes were 0.3 mm high, 30–40 mm wide and their vertical spacing was 2 mm. Chloride concentrations were systematically recorded at two depths in the wells, i.e., at the level corresponding to the E-horizon and B-horizon, and the level corresponding to the BC-horizon and C-horizon. Analysis of the concentrations implied that water in the wells changed fast due to a fast in-/outflow to/from the wells through the screen holes, water entering the wells was mainly irrigation water that by-passed the water in the soil matrix, and depth distributions of chloride concentrations in the wells reflected the vertical concentration distributions in the preferential flow domain in the surrounding soil profile [*Laine-Kaulio*, 2011]. Therefore, the concentration measurements represented the preferential flow domain. Data on the concentration status of the soil matrix were not available.

The irrigation caused an almost vertical saturation front that proceeded downslope along the centerline reaching one observation well after another. When the front reached a well, the water table in the well quickly rose up to the E-horizon. The water table did not reach the O layer, and no surface runoff was observed. Figure 2 shows the observed chloride concentration and water table along the centerline of the observation well field (cf. Figures 1b and 1c). The chloride plume is interpolated from the concentration measurements.

During the tracer irrigation, the migration velocity of the front was about 3 m h^{-1} within the initially wet, upper part of the experimental hillslope section (Figures 2a and 2b), and concentration levels corresponding to the irrigated tracer solution were found as far as 3 m from the irrigation source (Figure 2b). The irrigation was changed to tracer-free water at the same time as the saturation front reached the initially drier part of the slope. Thus, the migration velocity of the saturation front reduced to 0.5 m h^{-1} and concentration levels dropped remarkably at the same time (Figures 2c and 2d). Already 1 h after changing the

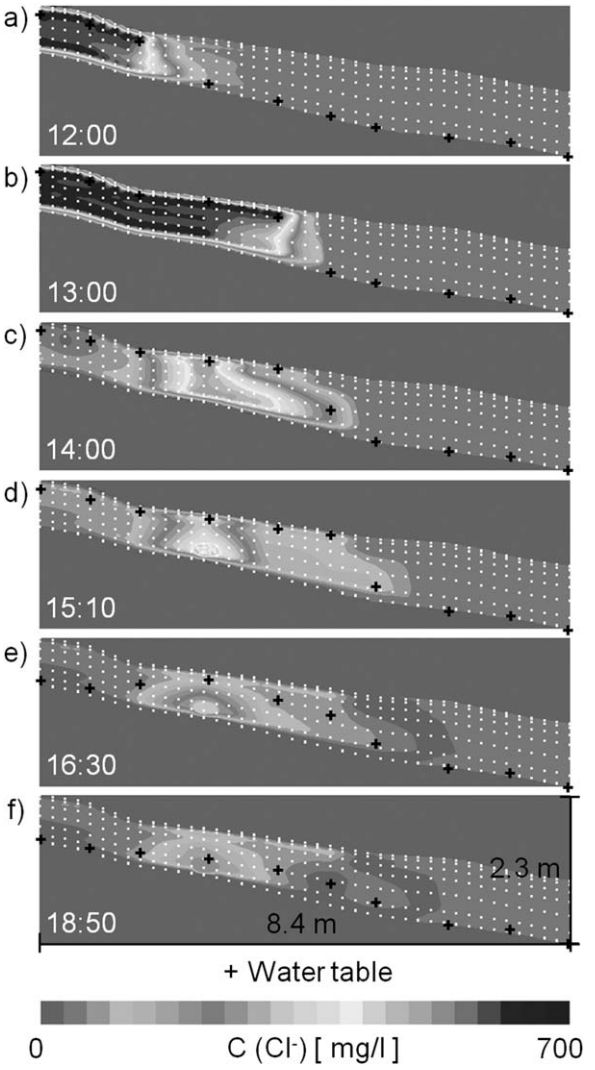

Figure 2. (a) Chloride concentration and water table in the soil profile along the experimental hillslope section at 12:00, 20 min after the initiation of tracer irrigation, (b) at 13:00, 1 h 20 min after the initiation of tracer irrigation, (c) at 14:00, 1 h after changing the irrigation to tracer-free water, (d) at 15:10, 2 h 10 min after changing the irrigation to tracer-free water, (e) at 16:30, 1 h 20 min after the irrigation was stopped, and (f) at 18:50, 3 h 40 min after the irrigation was stopped.

irrigation to tracer-free water, concentrations corresponding to the tracer-free water were found approximately 1 m from the irrigation source (Figure 2c).

During the dilution period, the maximum chloride concentration was recorded at a distance of about 2 m from the irrigation source (Figures 2c–2f). At the end of the observation period, the maximum concentration was 28% of the irrigated maximum value (Figure 2f). When the soil profile started to drain after irrigation, matrix water started to enter the observation wells as a consequence of the deactivation of preferential by-pass flow. Due to the falling water table, concentrations in the E-horizon and B-horizon at the end of the observation period were estimated based on the observed dilution velocity between 15:10 and 16:30. This introduces uncertainty into our characterization of the final chloride plume (Figure 2f).

2.3. Dual-Permeability Model

2.3.1. Mathematical Description of Water Flow

Simulation of water flow in the two pore domain soil system was based on the following partial differential equation (PDE) [*Gerke and van Genuchten*, 1993a]:

$$C^d(\partial h/\partial t)=\nabla(K\nabla H)\pm S\pm\Gamma_w \quad (1)$$

where C^d is the differential moisture capacity [L^{-1}], h is the pressure head [L], t is the time [T], K is the unsaturated hydraulic conductivity function [LT^{-1}], H is the hydraulic head [L], S is the sink/source from/into the system [$L^3L^{-3}T^{-1}$], and Γ_w is the exchange of water [$L^3L^{-3}T^{-1}$] between the two pore domains. The sign of Γ_w is positive when calculating flow in the soil matrix with equation (1) and negative when using the equation for the preferential flow domain. H can be calculated from h with the following equation:

$$H=h+z \quad (2)$$

where z is the elevation head [L]. When calculating the temporal change in pressure head at an arbitrary point, $\partial h/\partial t$ is equal to, and can be replaced with $\partial H/\partial t$ because the elevation head of the point does not change.

In the majority of studies on dual-permeability models, the model has been parameterized so that both pore domains alone covered the whole pore space in soil. This has led to the use of a scaling factor describing the ratio of the porosity of the preferential flow domain and total porosity in soil [e.g., *Gerke and van Genuchten*, 1993a, 1993b; *Šimůnek et al*., 2003; *Ray et al*., 2004; *Gerke et al*., 2007]. In the present study, the parameter values were directly scaled (section 2.4). Thus, no separate scaling factor was needed, and the exchange was calculated with the following equation:

$$\Gamma_w = \alpha_w (h_p - h_m) \tag{3}$$

where the subindices p and m refer to the preferential flow domain and to the soil matrix, respectively, and α_w is the first-order water transfer coefficient [$L^{-1}T^{-1}$] between the pore domains. α_w was determined following *Gerke and van Genuchten* [1993a]:

$$\alpha_w = \frac{\beta}{a^2} K_a \gamma_w \tag{4}$$

where β is a factor describing the geometry of the aggregates [–], a is the characteristic half width [L] of the matrix block, γ_w is an empirical coefficient [–], and K_a is the effective hydraulic conductivity [LT^{-1}] at the preferential flow domain-matrix interface. In the present study, a, β, and γ_w were lumped into one parameter α_{wl} [L^{-2}] to reduce the number of calibrated model parameters. Thus, α_w only consisted of one lumped coefficient α_{wl} and the average hydraulic conductivity between the pore domains K_a [*Ray et al.*, 1997]:

$$\Gamma_w = \alpha_{wl} K_a (h_p - h_m) \tag{5}$$

K_a was calculated as the arithmetic mean of hydraulic conductivities in the preferential flow domain and soil matrix.

Soil moisture θ [L^3L^{-3}] was connected to the pressure head using the model by *van Genuchten* [1980]:

$$\theta = \theta_R + \frac{\theta_S - \theta_R}{\left[1 + (\alpha|h|)^{\beta}\right]^{\left(1-\frac{1}{\beta}\right)}} \tag{6}$$

where θ_S and θ_R are the saturated and residual water contents [L^3L^{-3}], respectively, and α [L^{-1}] and β [–] are the shape parameters of the model. Following *van Genuchten* [1980], parameters α and β were used to link K to h using:

$$K = K_S S_e^{\left(\frac{1}{2}\right)} \left\{1 - \left[1 - S_e^{\left(\frac{1}{\beta}\right)}\right]^{\beta}\right\}^2 \tag{7}$$

where K_S is the saturated hydraulic conductivity [LT^{-1}] and S_e is the degree of saturation [–].

2.3.2. Mathematical Description of Solute Transport

The two pore domain version of the advection-dispersion equation [*Gerke and van Genuchten*, 1993a] was derived in the similar manner as the flow equation so that no scaling factor was needed. We used the following equation:

$$\frac{\partial(\theta C)}{\partial t} = \nabla[D\nabla(\theta C)] - v\nabla(\theta C) \pm S_s \pm \Gamma_s \tag{8}$$

where C is the concentration [ML^{-3}], D is the dispersion coefficient [L^2T^{-1}] that sums up diffusion and dispersion, v is the pore water velocity [LT^{-1}], S_s is the sink/source of solute from/into the system [MT^{-1}], and Γ_s is the term that describes the solute exchange [$ML^{-3}T^{-1}$] between the pore domains. The sign of Γ_s is positive when calculating transport in the soil matrix with the equation and negative when using the equation for the preferential flow domain.

The dispersion coefficient was calculated using the following equation [*Rausch et al.*, 2005]:

$$D_n = \alpha^* + \alpha_L \frac{v_L^2}{|v|} + \alpha_{T1} \frac{v_{T1}^2}{|v|} + \alpha_{T2} \frac{v_{T2}^2}{|v|} \tag{9}$$

where α^* is the constant diffusion term [L^2T^{-1}], α_L is the longitudinal dispersivity [L], α_T is the transverse dispersivity [L], v_L is the longitudinal flow velocity [L], v_{T1} and v_{T2} are the transverse flow velocities [LT^{-1}], and $|v|$ is the magnitude of the flow velocity [LT^{-1}]. $|v|$ was calculated using the following equation:

$$|v| = \sqrt{v_x^2 + v_y^2 + v_z^2} \tag{10}$$

where v_x is the flow velocity in the x direction, v_y in the y direction, and v_z in the z direction.

The numerical solution of equation (8) causes numerical dispersion:

$$d_n = v\Delta x/2 \tag{11}$$

where d_n is the numerical dispersion [L^2T^{-1}] and Δx is the spatial discretization step [L] of the numerical solution of the model (section 2.3.3). In order to remove the bias caused by numerical dispersion, numerical dispersion (equation (11)) was subtracted from the dispersion estimate (equation (9)) following *van Genuchten and Gray* [1978].

Gerke and van Genuchten [1993a] determined the solute exchange term Γ_s so that the exchange consisted of advective and diffusive solute exchange between the pore domains. In the present study, the exchange was assumed to be advection-driven during the short stormflow event, and the term was simplified to the following form:

$$\Gamma_S = (1-d)\alpha_{wl}K_a\left(H_p - H_m\right)C_p + d\alpha_{wl}K_a\left(H_p - H_m\right)C_m \tag{12}$$

where d is the flow direction switch [–] that has a value of zero when the flow direction is from the preferential domain to the soil matrix, and in the opposite case, d is one:

$$\begin{cases} d=0, & \left(H_p - H_m\right) \geq 0 \\ d=1, & \left(H_p - H_m\right) < 0 \end{cases} \tag{13}$$

2.3.3. Computational Implementation of the Model

The model equations were programmed into an object-oriented simulation model with Java so that the model can be run in a one or two pore domain mode. The spatial, numerical solution of the PDEs (equations (1) and (8)) relied on the control volume method [e.g., *Rausch et al*., 2005], and the temporal solution of the PDEs was implicit. The soil profile of the modeled hillslope section was divided into an unstructured grid of control volumes, and H and C were integrated over the control volumes at each time step. The implicit solution led into iterative calculation, where the solutions of PDEs formed a set of linear equations, which were solved using the tridiagonal Thomas' algorithm [e.g., *Wang and Anderson*, 1982]. The algorithm was based on solving the equations for a whole vertical column of grid cells at the same time with Gaussian elimination. In the lateral and horizontal directions, values of the variables in adjacent cells were taken from the previous iteration step.

The numerical solution was performed for each time step in the following order. First, the state of H was iterated with the Thomas algorithm for all vertical columns in the 3-D grid. When the iteration converged in all cells, the values of H were set as the initial values for the iteration of H in the next time step. A value of 10^{-4} cm was used as the convergence criterion for H. Second, values for the other variables, i.e., h, θ, C^d, and K were updated. The values of h were obtained from equation (2) and the values of θ from equation (6). Values of C^d were calculated using the difference quotient of soil moisture change versus pressure head change during each time step in each grid cell [*Karvonen*, 1988]:

$$C^d = \frac{\theta^{t+1} - \theta^t}{h^{t+1} - h^t} \tag{14}$$

The value of K in each grid cell was obtained from equation (7). When calculating flow and solute transport from one cell to another, arithmetic mean of the K values of the cells in question was used at the cell interface. Third, values of C were iterated with the Thomas algorithm, using a convergence criterion of 10^{-4} μg cm^{-3}. The procedure was repeated in the same manner at all time steps.

The calculation time step was 60 s, and the simulations were started from the beginning of the tracer irrigation. The modeled area was bounded at a distance of 1 m above the irrigation source and 2 m below the maximum distance that the chloride pulse reached during the experiment (Figures 1b and 2e). On both sides, the modeled area was extended 0.7 m wider than the irrigation tube. The soil and bedrock surfaces were interpolated from leveling data and soil depth data that were measured at the locations of the observation wells. The soil volume between the soil surface and bedrock was described as a sloping 3-D grid. The grid spacing was 0.2 m in the x and y directions, and the grid consisted of 25 cells in the x direction and 45 cells in the y direction. In the z direction, the soil profile was divided into five layers. The thicknesses of the

Table 3. *van Genuchten* [1980] Model Parameters Related to Average Water Retention Measurements and Air Capacity Measurements in the Preferential Flow Domain (*p*); van Genuchten Model Parameters for Average Water Retention Measurements and Average of Measured Saturated Hydraulic Conductivities in the Soil Matrix (*m*); Estimated Values of Dispersion Related Parameters in the Pore Domains[a]

Horizon, Domain	α (cm^{-1})	B	θ_R ($m^3\ m^{-3}$)	$N(pF)$	θ_S ($m^3\ m^{-3}$)	$N(\theta_S)$	K_S ($cm\ s^{-1}$)	$N(K_S)$	α^* ($cm^2\ s^{-1}$)	α_L (cm)	α_T (cm)
E_p	0.080	1.380	0	6	0.042	2			1.0E-06	50	5
B_p	0.039	1.375	0	6	0.025	2			1.0E-06	50	5
BC_p	0.032	1.440	0	2	0.019	2			1.0E-06	50	5
C_p	0.025	1.544	0	1	0.012	1			1.0E-06	50	5
E_m	0.013	1.861	0	5	0.282	2	6.2E-04	4	1.0E-06	5	0.5
B_m	0.008	1.600	0.019	5	0.307	2	9.8E-04	5	1.0E-06	5	0.5
BC_m	0.012	1.990	0.007	7	0.309	2	6.0E-04	4	1.0E-06	5	0.5
C_m	0.012	1.898	0	5	0.293	1	6.0E-04	4	1.0E-06	5	0.5

[a]*N* denotes sample size.

three topmost layers corresponded to the measured thicknesses of the E-horizon, B-horizon, and BC-horizon (Table 1), and the two bottom layers together covered the thickness of the C-horizon.

The soil and bedrock surfaces had a no flow boundary condition because no surface runoff was observed and the bedrock was nearly impermeable. The tracer irrigation was fed into the uppermost cell layer below the irrigation tube by the source terms S and S_s (equations (1) and (8)). Ninety percent of the irrigation was fed into the preferential flow domain and ten percent to the soil matrix. Test runs (not shown) indicated that fractioning of the irrigation to the two pore domains did not affect the results when a rather high value was used for the exchange coefficient α_{wl} (Table 5). The irrigation spread to every direction in soil in the 3-D model, and the fraction of irrigation that flowed downslope along the centerline of the observation well field was calculated with the model. The side boundaries (x and y direction) of the modeled area were set partly open using the Neumann-type boundary conditions [e.g., *Wang and Anderson*, 1982] so that fluxes out from the grid were allowed, but fluxes in were not allowed; the water or solute flux out from a cell at the boundary was set equal to the flux entering the cell in the direction normal to the boundary.

The model program was tested against analytical solutions of the flow equation [*Tracy*, 1995] and transport equation (*Ogata and Banks* [1961], as presented in *Fetter* [2001]), and the closure of the water and solute balances within the calculation domain were verified during simulations. Consistency of the solution with the chosen time step and grid spacing was confirmed by comparing the simulation results with results obtained with a shorter time step and denser spatial grid spacing. Development and implementation of the model program, as well as testing of the program, are presented in *Laine-Kaulio* [2011].

2.4. Principles for Model Parameterization and Evaluation

Table 3 shows the data available for model parameterization. Water retention data appointed to the preferential flow domain originate from soil cores with a substantial amount of macropores, whereas the water retention data, as well as the K_S values of the soil matrix originate from soil cores with a minor macropore fraction [*Laine-Kaulio*, 2011]. θ_S values of the preferential flow domain are measured values of air capacity in soil cores, corrected by the stone content data (cf. Table 1). Air capacity is the fraction of soil pore volume that drains from a saturated soil sample during 24 h, providing an estimate for effective macroporosity of soil (*Burger* [1922], cited in *Germann and Beven* [1981]). θ_S in the soil matrix is the difference between the total porosity of soil, corrected by the stone content, and the air capacity. α_L in the preferential flow domain is 10% of the total travel distance [e.g., *Spitz and Moreno*, 1996], and the value of α_T is 10% of the longitudinal dispersivity (e.g., *Klotz and Seiler* [1980], *Pickens and Grisak* [1980], as cited in *Rausch et al.* [2005]). The values of α_L and α_T in the soil matrix are 10% of their values in the preferential flow domain. The diffusivity α^* has a small nonzero value.

To limit the number of calibrated model parameters, the values of a subset of parameters were fixed to the values presented in Table 3. They were α, β, and K_S in the soil matrix, the sum of θ_S in the soil matrix, and θ_S in the preferential flow domain, i.e., the total pore space of soil, and parameters related to dispersion in both pore domains. Thus, the K_S values in the preferential flow domain, fractioning of the total θ_S of soil to θ_S in the preferential flow domain and θ_S in the soil matrix, as well as the value of α_{wl} between the pore

Table 4. van Genuchten Model Parameters for Average Water Retention Measurements, the Maximum Saturated Hydraulic Conductivities Obtained From Inverse Modeling of Water Table Levels in the Slope, and Estimated Values of Dispersion Related Parameters in the Total Soil Pore Space[a]

Horizon	α (cm^{-1})	β	θ_R ($m^3\ m^{-3}$)	$N(pF)$	θ_S ($m^3\ m^{-3}$)	$N(\theta_S)$	K_S ($cm\ s^{-1}$)	α^* ($cm^2\ s^{-1}$)	α_L (cm)	α_T (cm)
E	0.036	1.504	0	11	0.324	11	4.0E-02	1.0E-06	50	5
B	0.025	1.353	0	11	0.331	11	2.3E-02	1.0E-06	50	5
BC	0.018	1.708	0	9	0.328	9	1.5E-02	1.0E-06	50	5
C	0.013	1.813	0	6	0.305	6	1.0E-02	1.0E-06	50	5

[a]*N* denotes sample size.

domains were calibrated. α_{wl} was appointed a same value in the different soil horizons to reduce the number of calibrated parameter values. Because the exchange of water and solute between the pore domains was controlled both by α_{wl} and K_S values, different K_S values in the soil horizons yielded a different water and solute exchange.

The observed and simulated chloride concentrations provided clues to the origin of the water that flowed in the two pore domains, something that an examination of water tables could not do. Therefore, calibration and validation of the model were primarily based on comparing the measured chloride concentrations with the simulated ones, using two goodness of fit measures: the coefficient of determination, R^2, and the Nash-Sutcliffe efficiency coefficient, R_{NS} [for the definitions see, e.g., *Seibert*, 1999]. R^2 describes the proportion of the variance of the measured data that the modeled values explain, whereas R_{NS} is a dimensionless transformation of the sum of squared errors, and it accounts for the systematic bias in the modeled series [*Seibert*, 1999].

The concentration data at 13:00 and 15:10 (Figures 2b and 2d) were chosen for the model calibration because they represent the migration of the saturation front both in the wet (13:00) and in the dry (15:10) part of the slope, and they cover a longer distance downslope from the irrigation source than the time points 12:00 and 14:00 (Figures 2a and 2c). Data from 16:30 and 18:50 (Figures 2e and 2f) were not considered meaningful for calibration because the water table had started to draw down. The concentration data at 12:00, 14:00, 16:30, and 18:50 (Figures 2a, 2c, 2e, and 2f), as well as the water table data at all observation time points (Figures 2a–2f), were used for the model validation. After validating the model, different predictions produced by the model were investigated. At the end, the results were compared to the results obtained from a traditional one pore domain model and to the results from two pore domain simulations of a longer time period. The one pore domain model was parameterized with average water retention data and the highest K_S values calibrated with a groundwater model at the study site (Table 4) [*Laine-Kaulio et al.*, 2009; *Laine-Kaulio*, 2011].

3. Results

3.1. Calibration

Model calibration against the concentration data at 13:00 and 15:10 led to the parameter values presented in Table 5. The values of θ_S and α_{wl} were identified, but slightly different values of K_S produced equally good results. Figure 3 shows the simulation results related to the use of K_{S1} values and Figure 4 does so for the K_{S2} values (cf. Table 5). At 13:00, the K_{S1} values led to a steeper saturation front than the K_{S2} values, therefore the goodness of fit measures were higher for K_{S1} than for K_{S2} (Figures 3b and 4b). Because the K_{S1} values were lower than the K_{S2} values, the K_{S1} values led to a slower tracer infiltration into the deeper soils horizons.

Table 5. Calibrated Parameter Values of the Dual-Permeability Model: K_{S1} Values Produce the Highest Goodness of Fit at 13:00 and K_{S2} Values at 15:10[a]

Horizon, Domain	θ_R ($m^3\ m^{-3}$)	θ_S ($m^3\ m^{-3}$)	K_{S1} ($cm\ s^{-1}$)	K_{S2} ($cm\ s^{-1}$)	α_{WL} (cm^{-2})
E_p	0	0.070	8.0E-02	1.0E-01	0.001
B_p	0	0.035	3.0E-02	5.0E-02	0.001
BC_p	0	0.02	3.0E-03	7.0E-03	0.001
C_p	0	0.015	1.0E-03	2.0E-03	0.001
E_m	0	0.254			0.001
B_m	0.02	0.296			0.001
BC_m	0.008	0.308			0.001
C_m	0	0.290			0.001

[a]For simulations of a longer time period (Figures 7e, 7f, 7k, and 7l), θ_S in the soil matrix is 30% smaller.

At 15:10, the K_{S1} values produced a higher R_{NS} than the K_{S2} values (Figures 3d and 4d) because the K_{S1} values produced a better correspondence between the observed and simulated maximum concentration, located in the C-horizon at approximately 2 m from the irrigation source. The K_{S2} values led, for their part, into a higher R^2 than the K_{S1}

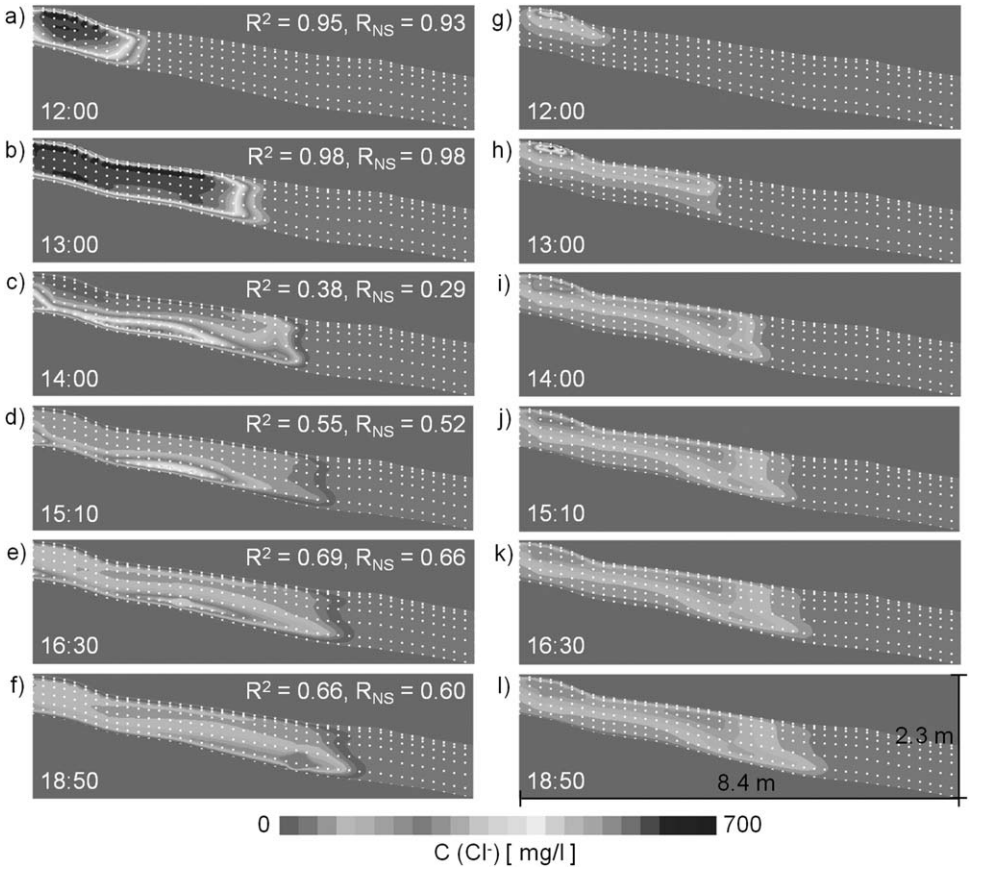

Figure 3. (a–f) Simulated chloride concentration in the preferential flow domain and (g–l) soil matrix with the parameterization presented in Table 5, using the K_{S1} values.

values because the K_{S2} values better reproduced the average chloride concentrations in the slope at 15:10. The higher K_{S2} values produced a higher exchange of water and solute between the pore domains than the lower K_{S1} values.

According to the calibration, the model was able to accurately simulate the chloride plume when it was migrating in the upper, wet part of the experimental hillslope section and the irrigation contained chloride (Figures 3b and 4b), but it overestimated the dilution of the plume when the irrigation was changed to tracer-free water and the plume reached the lower, dry part (Figures 3d and 4d).

3.2. Model Validation

Model validation against the concentration data at 12:00, 14:00, 16:30, and 18:50 was consistent with the model calibration: the model captured the observed plume when it was migrating in the wet part of the slope (Figures 3a and 4a), but it could not correctly simulate the dilution of the plume when it reached the dry part (Figures 3c and 4c). When the dilution continued, the goodness of fit slightly improved (Figures 3e, 3f and 4e, 4f).

Model validation against the water table data revealed that using the K_{S1} values, the model simulated the water tables very accurately at the measurement locations (Figures 5a–5f). Rather high R_{NS} values related to the results obtained with the K_{S2} values implied that this parameterization also captured the observed maximum levels of the water table, but was less successful in reproducing the average levels because the R^2 values were clearly lower (Figures 5g–5l). The main difference between the water tables related to the K_{S1} and K_{S2} values was that the K_{S1} values captured the shape of the plume with its sharp saturation front, which the K_{S2} values did not. Thus, validating the model against the water table data implied that the K_{S1} values produced better simulation results than the K_{S2} values.

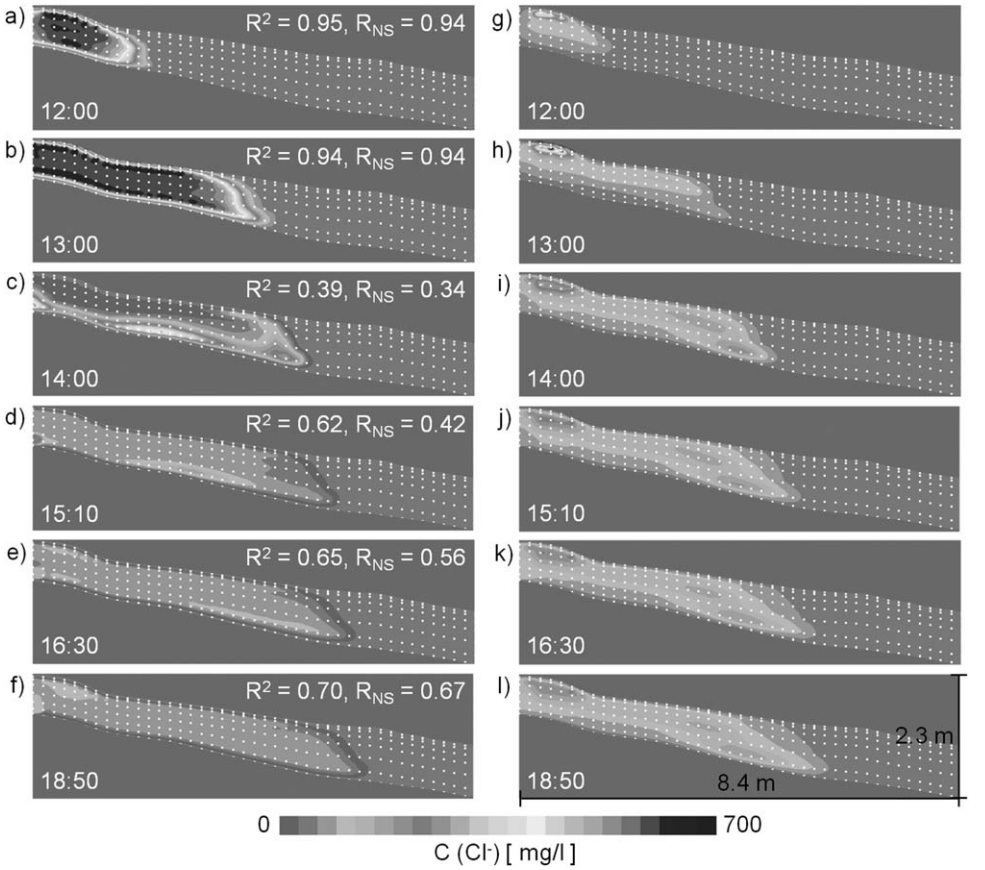

Figure 4. (a–f) Simulated chloride concentration in the preferential flow domain and (g–l) soil matrix with the parameterization presented in Table 5, using the K_{S2} values.

3.3. Predictions Provided by the Model

3.3.1. Concentration in the Soil Matrix

The simulated chloride concentrations in the soil matrix are presented in Figures 3g–3l and 4g–4l. The K_{S1} values produced higher chloride concentrations to the soil matrix than the K_{S2} values because the higher K_{S2} values led to a faster transport and spreading of chloride than the K_{S1} values. For instance at 13:00, the highest, simulated chloride concentration in the soil matrix, as produced by the K_{S1} values, was 570 mg L^{-1}, and the average concentration of the plume was 84 mg L^{-1} (Figure 3b). The K_{S2} values produced, for their part, a maximum concentration of 560 mg L^{-1} and an average concentration of 81 mg L^{-1} at 13:00 (Figure 4b).

Overall, concentrations in the soil matrix were low during the whole simulation period as compared to the concentrations in the preferential flow domain (Figures (3 and 4)). In the initially wet, upper part of the experimental hillslope section, a high amount of tracer-free preevent water was stored in the soil matrix and did not exit the domain. In the initially dry, lower part, both tracer-free event and preevent water saturated the soil matrix; the tracer-free event water was transported to the dry part via preferential flow domain in the E-horizon and B-horizon in the model.

3.3.2. Quantification of Lateral Tracer Transport and Tracer Exchange Between Pore Domains

The volume of the centerline grid cells was 4% of the total modeled soil volume. Considering the amount of chloride down the centerline of slope, of the chloride fed into the soil 1.8% was in the preferential flow domain and 2.3% in the soil matrix at 13:00, i.e., at the end of tracer irrigation (Figure 3b). At 15:10, i.e., the end of tracer-free irrigation, 0.4% of the chloride fed into soil was in the preferential flow domain and 2.8% in the soil matrix (Figure 3d). Even though more chloride was in the soil matrix than in the preferential flow domain in the centerline both at 13:00 and 15:10, the chloride concentration was higher in the preferential flow domain due to the smaller pore and water volume as compared to the soil matrix.

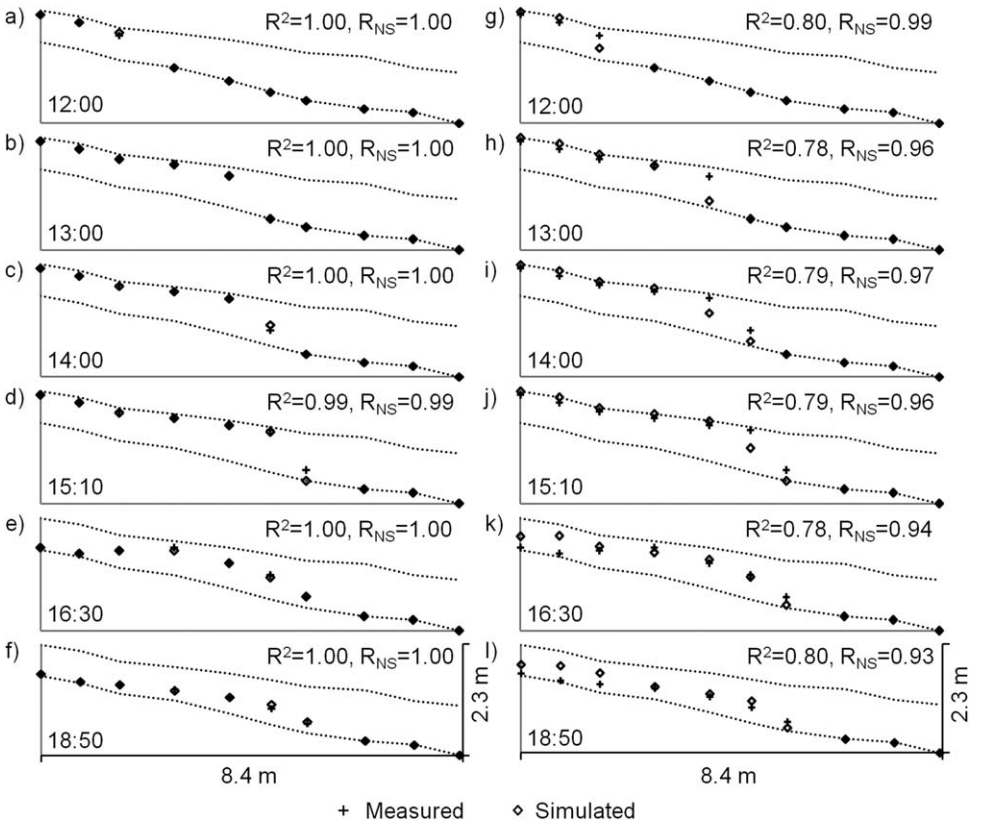

Figure 5. (a–f) Measured and simulated water table when using the K_{S1} and (g–l) K_{S2} values (Table 5).

The amount of chloride in the preferential flow domain in the centerline was 76.7% lower at 15:10 than at 13:00, and the amount of chloride in the soil matrix was 41.5% higher at 15:10 than at 13:00. Thus, 48.9% more chloride exited the preferential flow paths in the centerline than entered the soil matrix between 13:00 and 15:10. Chlorinated water did not only move from the preferential flow domain into the soil matrix in the lateral direction, but also spread into the soil pores on the sides of the centerline in the 3-D model. Considering the chloride mass balance in the whole 3-D calculation grid at 13:00, 41% of the irrigated chloride was in the preferential flow domain, 45% in the soil matrix, and 14% had flown outside the modeled soil block on its sides. At 15:10, 11% of the irrigated chloride resided in the preferential flow domain, 63% in the soil matrix, and 26% had flown outside the modeled soil block.

Figure 6 shows the simulated, lateral chloride transport and the chloride exchange between the soil matrix and the preferential flow domain in detail (cf. Figure 3). The numbers represent the amount of chloride that is transported from one model grid cell to another in the lateral direction, and from one pore domain to the other within one model grid cell in the different soil horizons at the distance of 2 m (Figures 6a–6f) and 4 m (Figures 6g–6l) from the irrigation source; the total pore volume in one grid cell varies from 1.2 dm^3 in the E-horizon to about 3.2 dm^3 in the C-horizon.

At 12:00, the plume had not yet reached the distance of 2 or 4 m (Figures 6a and 6g).

At 13:00, the plume had crossed the distance of 2 m, and the soil profile was saturated up to the E-horizon. Lateral flow in the preferential flow domain was the dominating transport mechanism, delivering 140 times more chloride down the slope than the soil matrix (Figure 6b).

At 14:00, the plume had also reached the 4 m mark at the initially drier part of the slope. At this distance, about the same amount of chloride migrated in the lateral direction in the preferential flow domain as was transported from the preferential flow domain into the soil matrix in each layer of the entire soil profile (Figure 6i), demonstrating the saturation process of soil and the simultaneous activation of lateral

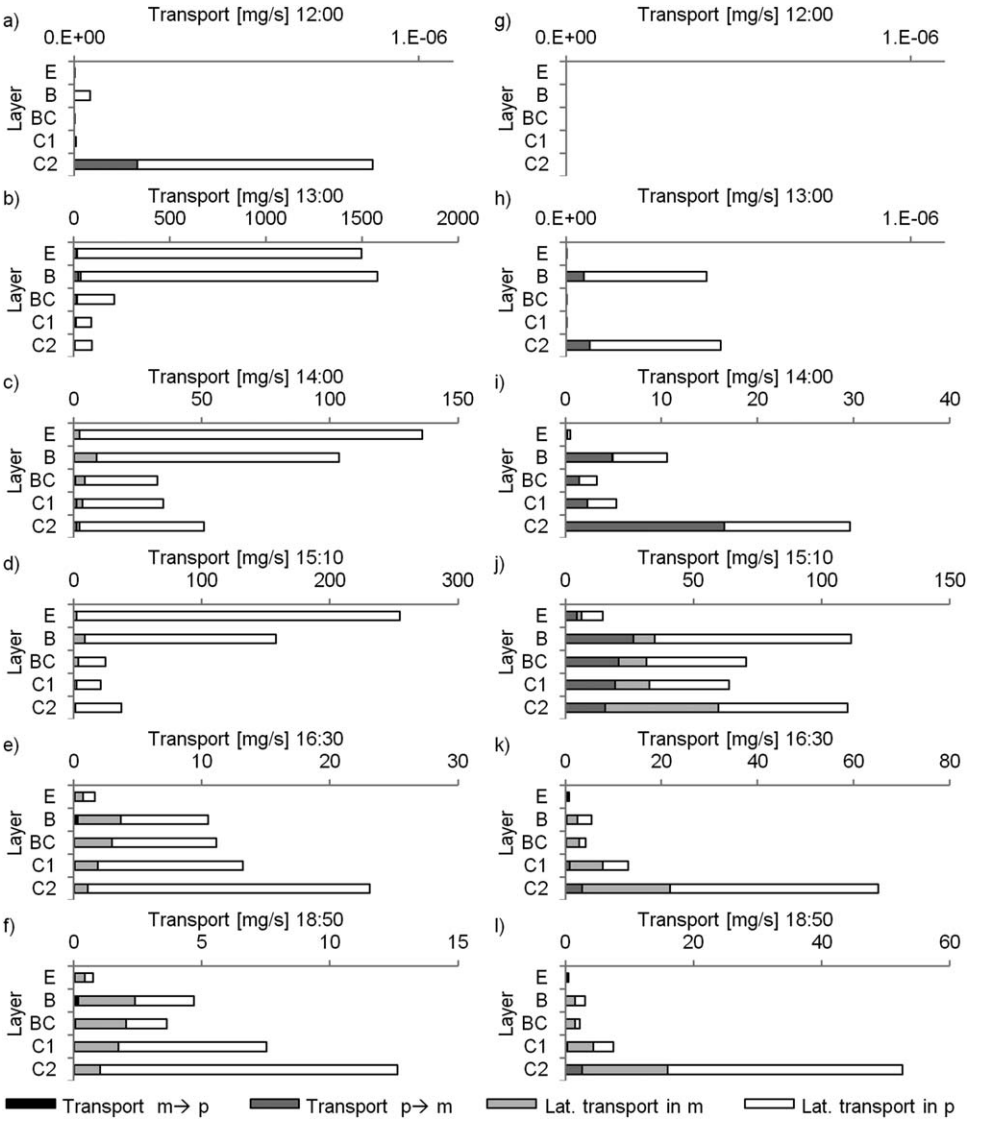

Figure 6. (a–f) Lateral chloride transport in the preferential flow domain, *p*, and in the soil matrix, *m*, as well as chloride transport (i.e., exchange) between the pore domains at the distance of 2 m and (g–l) 4 m from the irrigation source in the different soil horizons in the centerline grid cells.

subsurface stormflow near the leading edge of the saturation front. At the distance of 2 m, the amount of chloride transported by lateral preferential flow reduced to less than a tenth in the E-horizon and B-horizon and to a half in the C-horizon, as compared to the amounts at 13:00 (Figures 6b and 6c). This reduction was due to the reduction of migration velocity of the saturation front, and due to the change of irrigation into tracer-free water an hour earlier.

At 15:10, soil was saturated up to the B-horizon at the distance of 4 m. Due to the rather low migration velocity of the saturation front near its leading edge, lateral chloride transport in the preferential flow domain did not clearly dominate the subsurface flow processes (Figure 6j). Lateral chloride transport in the soil matrix was as high as the lateral transport in the preferential flow domain in the C-horizon and about 6% of the lateral chloride transport in the preferential flow domain in the B-horizon. However, the amount of chloride transported in the lateral direction in the preferential flow domain at 15:10 increased when compared to the amount at 14:00 (Figures 6c, 6d, 6i, and 6j). At the distance of 2 m, the chloride increase resulted from the chloride remains in the last irrigation tank, and at the distance of 4 m from the increase in lateral flow velocity.

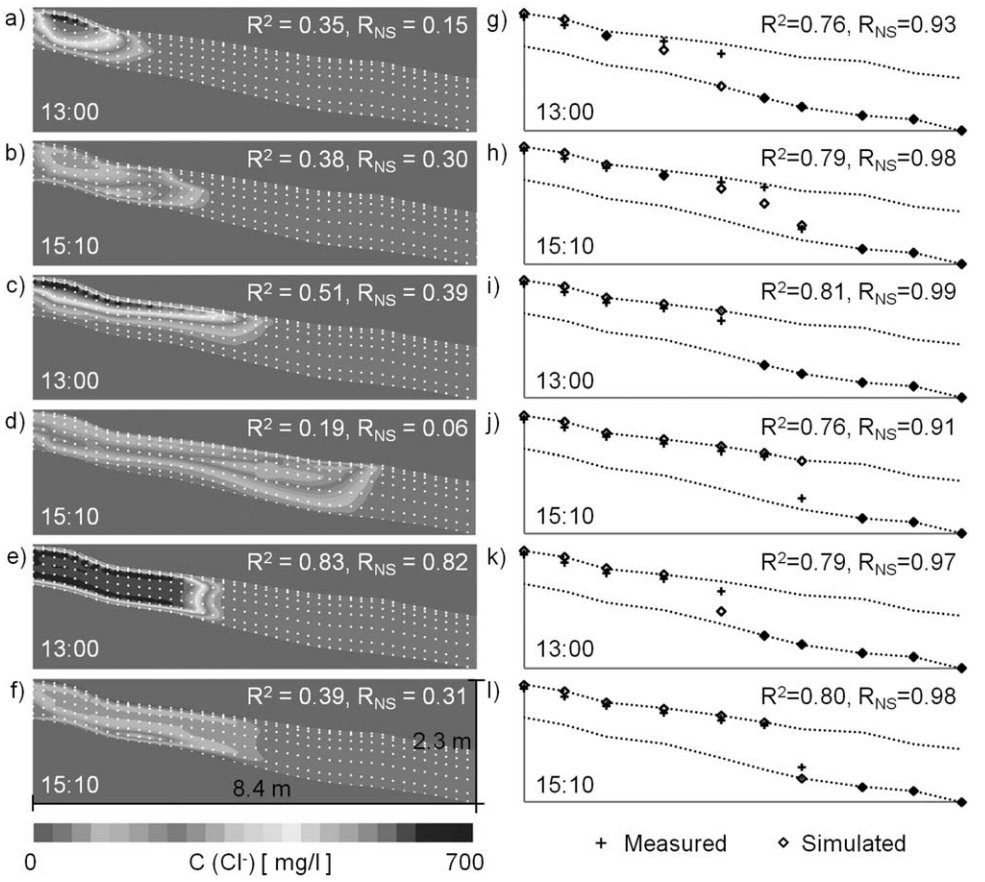

Figure 7. (a, b, g, and h) Reference results from one pore domain simulations when using the parameterization of Table 4. (c, d, i, and j) Reference results from one pore domain simulations when halving the θ_S values (Table 4) and replacing the K_S values (Table 4) with the K_{S1} values of Table 5. (e, f, k, and l) Results from two pore domain simulations when using the parameterization of Table 5 with the K_{S1} values and when starting the simulation from the beginning of the initial irrigation period.

At 16:30 (and 18:50), 1 h 20 min (and 3 h 40 min) after irrigation stopped, the slope drained, and the water table withdrew toward the bedrock. Consequently the fraction of lateral chloride transport in the soil matrix increased in relation to the lateral transport in the preferential flow domain at the 2 m mark (Figures 6e and 6f). The fraction of chloride transport in the soil matrix was larger in the uppermost soil horizons where the water table was no longer present. Draining of the slope also induced chloride transport from the soil matrix into the preferential flow domain, particularly in the B-horizon (Figures 6e and 6f). At the distance of 4 m, the upper soil horizons drained quicker than at the 2 m mark, and a greater fraction of lateral flow in the slope took place near the bedrock as compared to the upper soil horizons (Figures 6k and 6l).

3.4. Reference Simulations With a Traditional One Pore Domain Model

The model was run in a traditional one pore domain mode using the default parameterization presented in Table 4. As presented as an example for time points 13:00 and 15:10, the one pore domain model underestimated the spreading of the chloride plume (Figures 7a and 7b) and the water table (Figures 7g and 7h) even though the highest measured values of the initial soil moisture content were used (Table 2). Means to increase the migration velocity of the plume were to increase the K_S values and to lower the θ_S values in the model. When the K_S values (Table 4) were multiplied by 1.5, the model still produced similar plumes than those in Figures 7a and 7b. This was because the soil did not saturate in the E-horizon and B-horizon when the higher K_S values were used, and the migration velocity of the plume did not thereby increase.

When the θ_S values (Table 4) were multiplied by 0.5, and the K_S values (Table 4) were replaced with the calibrated K_{S1} values of the preferential flow domain (Table 5), the chloride plume spread further downslope (Figures 7c and 7d) and the form of the saturation front got sharper (Figures 7i and 7j). However, the goodness of fit only improved at 13:00 (Figures 7c and 7i), but not at 15:10 (Figures 7d and 7j). Thus, halving the

θ_S values improved the simulated migration velocity of the saturation front when the plume was flowing in the initially wet part of the experimental hillslope section (Figure 7i), but when the plume reached the initially dry part, the migration velocity was too fast (Figure 7j).

3.5. Simulation of a Longer Time Period

Simulation of a longer time period was conducted by starting a two pore domain simulation from the beginning of the initial irrigation period (section 2.2). The simulation was run with the calibrated parameter values presented in Table 5, using the K_{S1} values. The correspondence between the simulated and observed chloride concentrations was lower than in the simulations of the tracer experiment only, as shown in Figures 7e and 7f at time points 13:00 and 15:10. The modeled migration velocity of the plume did not reach the observed level (Figures 7k and 7l).

Test runs (not shown) verified that increasing the initial moisture status of soil even above the measured maximum could not increase the flow velocity to the observed level. Also, increased K_S values in the preferential flow domain could not produce high enough flow velocities because the soil lo longer saturated and the theoretical, maximum, lateral flow velocity was not reached. Only the use of lowered θ_S values could produce the observed migration velocity of the plume. Using 30% lower θ_S values of the soil matrix than presented in Table 5 produced results similar to those presented in Figures 3 and 5a–5f; the R^2 and R_{NS} values were only 0.01 units lower than in Figure 3 at every time point except for 14:00 and 18:50 when the R_{NS} values were 0.04 units higher.

4. Discussion

4.1. Flow and Transport Processes During the Experiment

4.1.1. Initiation of the Event

Previous experimental work has shown that preferential flow is dependent on the initial soil moisture content and on the intensity and duration of rainfall [*Jarvis*, 2007]. Furthermore, initiation of macropore flow and water exchange between macropores and the soil matrix have a marked influence on the resulting runoff generation processes [*Weiler and Naef*, 2000]. At the beginning of our experiment, the hillslope was wet but not saturated in the vicinity of the irrigation source. At the onset of tracer irrigation, most event water entered the preferential flow domain directly, and displaced the preevent water to the surrounding macropores and into the soil matrix. This is consistent with other field-based experiments that have shown that in coarse-textured soils, the soil matrix saturates via macropores before preferential flow in the macropores initiates [*Aubertin*, 1971; *Weiler and Naef*, 2003]. The dual-permeability model captured the early stages of the stormflow event.

4.1.2. Transport in Wet Soil During Tracer Irrigation

Our experiment was in contrast to events with low rainfall and infiltration intensities that can mobilize large amounts of preevent water that produce runoff [*Bishop et al*., 2004]. The tracer irrigation generated lateral subsurface stormflow that was dominated by preferential by-pass flow of chlorinated event water. *Weiler and Naef* [2000] and *Kienzler and Naef* [2008] have shown that when infiltrating precipitation feeds directly into preferential flow paths, lateral subsurface stormflow responds quickly with correspondingly low preevent water fractions. The rapid response of the observed water tables and chloride concentrations to the tracer irrigation, along with the fast, lateral by-pass flow of chlorinated event water in the initially wet soil suggested that individual, short macropore segments rapidly self-organized into larger preferential flow systems [cf. *Sidle et al*., 2001]. The model mimicked the lateral transport dominated by by-pass flow.

4.1.3. Dilution and Draining Phase

Changing the irrigation into tracer-free water rapidly flushed chloride from the preferential flow domain in the E-horizon and B-horizon due to the ongoing fast by-pass flow, but chloride was stored in the preferential flow domain in the BC-horizon and C-horizon at a distance of about 2 m from the irrigation source. This remaining chloride and its slow dilution indicated that the macropore volume, density, and connectivity, as well as the lateral flow velocity, were low in the lower soil horizons. Preferential flow paths have not been detected at the soil-bedrock interface in the midslope area of the Kangaslampi slope [*Laine-Kaulio*, 2011].

Low chloride concentrations in the whole soil profile farther downslope showed that water entering the soil pores in the initially dry part of the experimental slope section originated from lateral by-pass flow in the

upper soil horizons, indicative of transmissivity feedback [*Bishop*, 1991; *Bishop et al*., 2011]. The transmissivity feedback phenomenon was also shown by the hydraulic conductivities and tracer transport rates that increased nonlinearly from the C-horizon to the E-horizon. The model simulated the transmissivity feedback phenomenon, but it overestimated the dilution velocity of the tracer plume in the most conductive upper soil horizons after changing the irrigation to tracer-free water. The model did thereby not reproduce the observed dilution dynamics of the plume. The simultaneous withdrawal of the water table was correctly simulated by the model. The E-horizon and B-horizon drained quickly, whereas flow and transport in the C-horizon were fed by water draining from the upper soil horizons and from upslope.

4.2. Model Structural Compatibility

Our model accurately simulated the water table levels during the entire observation period (Figures 5a–5f), as well as the tracer concentrations in the preferential flow domain when the plume was migrating in the initially wet part of the slope (Figures 3a–3f). Shortcomings related to the simulation of the dilution phase implied that we oversimplified the mathematical description of water and solute exchange between the two pore domains in our model. We used the same value for α_{wl} in all soil horizons, and simplified the calculation of solute exchange [*Gerke and van Genuchten*, 1993a] to only account for advective exchange. In addition, parameter values that only changed with depth did not account for the unknown, exact 3-D spatial variability of highly heterogeneous till.

To alter the simulated dilution in future studies, different α_{wl} values should be calibrated for the different soil horizons, and different definitions for the exchange term that also describe the diffusive exchange between the pore domains, and that rely on the moisture status of the more dynamic preferential flow domain [e.g., *Ray et al*., 2004; *Gerke et al*., 2007] need to be tested. Including the diffusive exchange in the model is particularly important for longer simulations of natural, lower intensity rainfall-runoff events, as shown by *Gerke and Köhne* [2004] for an agricultural field in Germany. Test runs (not shown) indicate that activating the diffusive exchange [cf. *Gerke and van Genuchten*, 1993a] in our model does not alone cause clear improvements in the simulation results because of the short observation period of about 7 h. For instance, using the maximum value of the diffusive solute exchange coefficient presented in *Gärdenäs et al*. [2006] improve the R^2 value at the very worst performing time point in our simulations (cf. Figure 3c) only by 0.01 and the R_{NS} value only by 0.05 units.

Despite the limitations in simulating the dilution dynamics, the dual-permeability model mimicked the observed event better than a one pore domain model (Figures 3 and 7a–7d, 7g–7j). None of the irrigated tracer could migrate rapidly downslope in the total soil pore space in the one pore domain model. Attempts to simulate the observed, fast spreading of the tracer with the one pore domain model necessitated lowering the total θ_S values of soil, still feeding all of the irrigated water volume unrealistically to the halved soil pore space. Yet, the one pore domain model could not mimic the observed solute concentrations because tracer-free preevent water could not exit the single pore domain during the tracer-irrigation, and chlorinated water could not exit the single pore domain after changing the irrigation to tracer-free water. Due to the mismatch between observed and simulated migration velocities and concentration dynamics of the tracer plume, the one pore domain approach could neither describe the average tracer transport of the two pore domains, nor the transport in the preferential flow domain only.

4.3. Effect of Parameterization on the Model Behavior

The parameterization principle used in this study differed from approaches used in earlier applications of similar physically based models at agricultural sites [e.g., *Gärdenäs et al*., 2006; *Köhne et al*., 2006; *Vogel et al*., 2007; *Gerke et al*., 2007; *Dušek et al*., 2010]. These studies have commonly used fixed parameter values obtained from soil core analyses of, for instance, K_S. In our case, calibrating the K_S and θ_S values of the preferential flow domain together with the α_{wl} value between the pore domains against the chloride concentration data revealed the sensitivity of the model to these interacting parameters. The 1-D, two pore domain S1D model [*Dušek et al*., 2010] was found to be sensitive to this same parameter triplet when simulating the discharge from a forested, sandy loam hillside in the Czech Republic [*Dohnal et al*., 2012].

Small θ_S and high K_S values of the preferential flow domain ensured, in combination with a moderate α_{wl} value, a high migration velocity for the saturation front. The concentration levels at different depths controlled the depth distribution of the θ_S and K_S values. Adjusted values of θ_S and α_{wl} were, for their part,

crucial for simulating the observed, high concentrations during the tracer irrigation and for increasing the dilution velocity when the irrigation was changed to tracer-free water. The simulations emphasized the sensitivity of the model to the K_S values of the preferential flow domain. The inclusion of the initial irrigation period into simulation further revealed the importance of determining a reliable estimate for the total θ_S.

The ability to identify parameter values of two pore domain models has been problematic in previous studies with few clear suggestions for what kind of experimental data would support the identifiability of the underlying model [e.g., *Arora et al*., 2012]. Our results indicate that tracer data facilitate the model calibration, and that data from a manipulation experiment provide means to test model structures (as proposed by *Kirchner* [2006]). Data on the soil moisture dynamics and on the solute concentrations in soil matrix are needed to further assess the model parameterization and structure. For instance, additional data are needed to assess the parameter values that were fixed in the present study, and to evaluate the suitability of the model to other events and sites.

4.4. Analysis of Calibrated Parameter Values

4.4.1. Saturated Hydraulic Conductivity

The calibrated K_S values of the preferential flow domain (Table 5) were higher than those determined for till soil cores for the nearby study catchment of Kangasvaara [*Möttönen*, 2000], or for soil core analyses of Finnish tills in general [e.g., *Airaksinen*, 1978] as well as for Scandinavian tills with a variety of field methods [*Lind and Lundin*, 1990]. None of the laboratory or field methods correspond to the hillslope section scale of the present study. We note that K_S has been found to be scale dependent [e.g., *Jenssen*, 1990; *Buttle and House*, 1997]. The calibrated K_S values of the preferential flow domain decreased rapidly with depth and were strongly controlled by the macroporous soil structure [cf. *Lind and Lundin*, 1990].

4.4.2. Saturated Soil Moisture Content

The calibrated θ_S values of the preferential flow domain (Table 5) were higher than the measured air capacities (Table 3) and smaller than effective porosities of forest soils reported by others [e.g., *Dunn et al*., 2007]. The total θ_S values in the different soil horizons were fixed, and their values corresponded with the porosities reported for Finnish tills [*Airaksinen*, 1978]. However, including the initial irrigation period in the two pore domain simulation indicated that the average, measurement-based, total θ_S values of soil were too high. Capturing of the observed tracer plume in that case with the model required lowering the θ_S values of soil matrix by 30%. This led to a total, average θ_S of about 0.24 in the E-horizon, B-horizon, and BC-horizon, and 0.22 in the C-horizon. These values were within the range of variation of the measured θ_S values (Table 1). It is also important to notice that our θ_S measurements originated from soil cores that were saturated in a laboratory. Such values have been found 30% larger than θ_S values measured in the field conditions for same soil material, implying that soil cores may produce unreliable θ_S estimates due to sample manipulations [*Vakkilainen*, 1982].

4.4.3. Water Exchange Coefficient Between Pore Domains

The optimal value for α_{wl} was found by simultaneously adjusting the K_S and θ_S values of the preferential flow domain. In the HYDRUS model [e.g., *Šimůnek et al*., 1999, 2003], it is possible to choose the same definition for the water exchange as was used in the present study, and reference values are available for α_{wl} from agricultural sites: *Köhne et al*. [2006] obtained a α_{wl} value of 0.0035 cm^{-2} as a result of inverse modeling when simulating 1-D flow in loam and sand soil columns, and 1-D bromide transport in a tile-drained, loamy field in Germany, and *Gärdenäs et al*. [2006] set the α_{wl} value to 0.004 cm^{-2} for simulations of 2-D pesticide transport from a tile-drained, loamy till soil field in Sweden. These values are about 4 times higher than the value obtained in the present study, i.e., 0.001 cm^{-2}. According to test runs (not shown), a 10 times larger α_{wl} value, i.e., 0.01 cm^{-2}, caused minor changes to our simulation results, but a 10 times smaller α_{wl} value, i.e., 0.0001 cm^{-2}, led to poor simulation results. Thus, studies of *Köhne et al*. [2006] and *Gärdenäs et al*. [2006], as well as our study, suggest a similar value for α_{wl}.

5. Conclusions

This study focused on performing a parallel and coupled 3-D simulation of flow and solute transport in the preferential flow paths and soil matrix within a boreal forested hillslope. A hillslope section-scale tracer experiment was used to describe the temporal dynamics of tracer concentration in the preferential flow domain, as well as the water table dynamics along the study slope during the initiation, steady state, and

recession stages of an irrigation pulse. Fixing the values of most model parameters and calibrating the model against the tracer data made it possible to find a rather unambiguous set of parameter values. It also allowed us to assess the structural compatibility of the two pore domain model within the framework of the parameterization. While the field data described the lateral migration of the tracer plume in the preferential flow domain, the model produced a description of flow and transport in and between the two pore domains.

The two pore domain model provided a better description of the observed event than a traditional one pore domain model. The one pore domain model could neither describe the average tracer transport of the two pore domains, nor the transport in the preferential flow domain only. The dual-permeability model was able to accurately reproduce the internal processes associated with each of the stages of the observed event except for the dilution dynamics of the tracer plume. Lateral subsurface stormflow and solute transport at the slope were controlled by transmissivity feedback and preferential flow processes. Using our own model made it possible to directly access the source code and examine separate water and solute fluxes between the model grid cells and pore domains. In future studies using our model, it will be possible to define and test different calculation routines for, e.g., the solute exchange term.

Finally, the simulations presented in this paper are promising for further use of Richards' equation-based dual-permeability models in forest sites. For instance, assessment of water quality effects of forestry relies on a holistic understanding of element cycles, including the ability of soil to retain, release and transport nutrients in transient moisture conditions. Using new information on sorption and transport processes of nutrients in the preferential flow paths and in the soil matrix of forest soil [e.g., *Backnäs et al*., 2012], and linking a detailed decomposition model [e.g., *Laine-Kaulio et al*., 2014] into an advanced two pore domain model, provide hope for new insights into nutrient transport in forest soils.

Acknowledgments

We thank P. Vakkilainen and A. Laurén for valuable feedback, K. Janzen for proofreading, and the MVTT (Maa- ja vesitekniikan tuki ry.), the Emil Aaltonen Foundation, and the Department of Civil and Environmental Engineering, Aalto University, for financial support. Comments provided by the Editor, Associate Editor, and three anonymous reviewers are greatly acknowledged. Data used in modeling (Figure 2) can be requested from the corresponding author. The model program has not been released.

References

Airaksinen, J. (1978), *Maa- ja pohjavesihydrologia*, Kirjapaino Osakeyhtiö Kaleva, Oulu, Finland.

Allaire, S. E., S. Roulier, and A. J. Cessna (2009), Quantifying preferential flow in soils: A review of different techniques, *J. Hydrol.*, *378*, 179–204, doi:10.1016/j.jhydrol.2009.08.013.

Arora, B., B. P. Mohanty, and J. T. McGuire (2012), Uncertainty in dual permeability model parameters for structured soils, *Water Resour. Res.*, *48*, W01524, doi:10.1029/2011WR010500.

Aubertin, G. M. (1971), Nature and extent of macropores in forest soils and their influence on subsurface water movement, *U.S.D.A. For. Serv. Res. Pap. NE-192*, 33 pp.

Bachmair, S., and M. Weiler (2011), New dimensions of Hillslope Hydrology, in *Forest Hydrology and Biogeochemistry: Synthesis of Past Research and Future Directions, Ecol. Stud. Ser.* vol. 216, edited by D. F. Levia et al., chap. 23, pp. 455–481, Springer, Netherlands, doi: 10.1007/978-94-007-1363-5_23.

Backnäs, S., H. Laine-Kaulio, and B. Kløve (2012), Phosphorus forms and related soil chemistry in preferential flowpaths and the soil matrix of a forested podzolic till soil profile, *Geoderma*, *189–190*, 50–64, doi:10.1016/j.geoderma.2012.04.016.

Beven, K. J., and P. Germann (1982), Macropores and water flow in soils, *Water Resour. Res.*, *18*(5), 1311–1325.

Beven, K. J., and P. Germann (2013), Macropores and water flow in soils revisited, *Water Resour. Res.*, *49*, 3071–3092, doi:10.1002/wrcr.20156.

Bishop, K. H. (1991), Episodic increase in stream acidity, catchment flow pathways and hydrograph separation, Doctoral dissertation, Univ. of Cambridge, Cambridge, U. K.

Bishop, K., J. Seibert, S. Köhler, and H. Laudon (2004), Resolving the Double Paradox of rapidly mobilized old water with highly variable responses in runoff chemistry, *Hydrol. Processes*, *18*, 185–189, doi:10.1002/hyp.5209.

Bishop, K., J. Seibert, L. Nyberg, and A. Rodhe (2011), Water storage in a till catchment. II: Implications of transmissivity feedback for flow paths and turnover times, *Hydrol. Processes*, *25*, 3950–3959, doi:10.1002/hyp.8355.

Burger, H. (1922), Physikalische Eigenschaften von Wald- und Freilandböden, *Mitt. Schweiz. Zentral. Forstl. Vers.*, *13*(1), 1–221.

Buttle, J. M., and D. A. House (1997), Spatial variability of saturated hydraulic conductivity in shallow macroporous soils in a forested basin, *J. Hydrol.*, *203*, 127–142.

Cajander, A. K. (1949), Forest types and their significance, *Acta For. Fenn.*, *56*(5), 1–71.

Dohnal, M., T. Vogel, M. Sanda, and V. Jelínková (2012), Uncertainty analysis of a dual-continuum model used to simulate subsurface hillslope runoff involving oxygen-18 as natural tracer, *J. Hydrol. Hydromech.*, *60*(3), 194–205, doi:10.2478/v10098-012-0017-0.

Dunn, S. M., J. J. McDonnell, and K. B. Vache (2007), Factors influencing the residence time of catchment waters: A virtual experiment approach, *Water Resour. Res.*, *43*, W06408, doi:10.1029/2006WR005393.

Dušek, J., T. Vogel, L. Lichner, and A. Čipáková (2010), Short-term transport of cadmium during a heavy-rain event simulated by a dual-continuum approach, *J. Plant Nutr. Soil Sci.*, *173*, 536–547, doi:10.1002/jpln.200800281.

Dušek, J., T. Vogel, M. Dohnal, and H. H. Gerke (2012), Combining dual-continuum approach with diffusion wave model to include a preferential flow component in hillslope scale modeling of shallow subsurface runoff, *Adv. Water Resour.*, *44*, 113–125, doi:10.1016/j.advwatres.2012.05.006.

Ebel, B. A., K. Loague, D. R. Montgomery, and W. E. Dietrich (2008), Physics-based continuous simulation of long-term near-surface hydrologic response for the Coos Bay experimental catchment, *Water Resour. Res.*, *44*, W07417, doi:10.1029/2007WR006442.

Espeby, B. (1989), Water flow in a forested till slope: Field studies and physically based modelling, Doctoral dissertation, *Rep. Trita-Kut 1052*, Dep. of Land and Water Resour., R. Inst. of Technol., Stockholm.

Fetter, C. W. (2001), *Applied Hydrogeology*, 4th ed., Prentice Hall, Upper Saddle River, N. J.
Food and Agriculture Organization (FAO) (1988), Food and Agriculture Organization FAO/UNESCO Soil Map of the World (revised legend), *World Resour. Rep. 60*, Rome. Reprinted as Technical Paper 20, 1989. ISRIC Wageningen.
Gärdenäs, A. I., J. Šimůnek, N. Jarvis, and M. Th. van Genuchten (2006), Two-dimensional modelling of preferential water flow and pesticide transport from a tile-drained field, *J. Hydrol.*, *329*, 647–660, doi:10.1016/j.jhydrol.2006.03.021.
Gerke, H. H. (2006), Preferential flow descriptions for structured soils, *J. Plant Nutr. Soil Sci.*, *169*, 382–400.
Gerke, H. H., and M. Th. van Genuchten (1993a), A dual-porosity model for simulating the preferential movement of water and solutes in structured porous media, *Water Resour. Res.*, *20*(2), 305–319.
Gerke, H. H., and M. Köhne (2004), Dual-permeability modeling of preferential bromide leaching from a tile-drained glacial till agricultural field, *J. Hydrol.*, *289*, 239–257, doi:10.1016/j.jhydrol.2003.11.019.
Gerke, H. H., and M. Th. van Genuchten (1993b), Evaluation of a first-order water transfer term for variably saturated dual-porosity flow models, *Water Resour. Res.*, *29*(4), 1225–1238.
Gerke, H. H., J. Dušek, T. Vogel, and J. M. Köhne (2007), Two-dimensional dual-permeability analyses of a bromide tracer experiment on a tile-drained field, *Vadose Zone J.*, *6*(3), 651–667, doi:10.2136/vzj2007.0033.
Germann, P., and K. Beven (1981), Water flow in soil macropores. III: A statistical approach, *J. Soil Sci.*, *32*(1), 31–39.
Hopp, L., and J. J. McDonnell (2009), Connectivity at the hillslope scale: Identifying interactions between storm size, bedrock permeability, slope angle and soil depth, *J. Hydrol.*, *376*, 378–391, doi:10.1016/j.jhydrol.2009.07.047.
Iorgulescu, I., K. J. Beven, and A. Musy (2005), Data-based modelling of runoff and chemical tracer concentrations in the Haute-Menthue (Switzerland) research catchment, *Hydrol. Processes*, *19*, 2557–2574, doi:10.1002/hyp.5731.
James, A. L., J. J. McDonnell, H. J. Tromp-van Meerveld, and N. E. Peters (2010), Gypsies in the palace: Experimentalist's view on the use of 3-D physics-based simulation of hillslope hydrological response, *Hydrol. Processes*, *24*, 3878–3893, doi:10.1002/hyp.7819.
Jansson, P. E., and S. Halldin (1979), Model for the annual water and energy flow in a layered soil, in *Comparison of Forest and Energy Exchange Models*, edited by S. Halldin, pp. 145–163, Soc. for Ecol. Modell., Copenhagen.
Jansson, P. E., and S. Karlsberg (2001), *Coupled Heat and Mass Transfer Model for Soil-Plant-Atmosphere Systems, User's Manual*, Div. of Land and Water Resour., KTH, Stockholm.
Jansson, C., B. Espeby, and P. E. Jansson (2005), Preferential water flow in a glacial till soil, *Nord. Hydrol.*, *36*(1), 1–11.
Jarvis, N. (2007), A review of non-equilibrium water flow and solute transport in soil macropores: Principles, controlling factors and consequences for water quality, *Eur. J. Soil Sci.*, *58*, 523–546, doi:10.1111/j.1365-2389.2007.00915.x.
Jenssen, P. D. (1990), Methods for measuring the saturated hydraulic conductivity of tills, *Nord. Hydrol.*, *21*, 95–106.
Karvonen, T. (1988), A model for predicting the effect of drainage on soil moisture, soil temperature and crop yield, Doctoral thesis, Helsinki Univ. of Technol., Espoo, Finland.
Kienzler, P. M., and F. Naef (2008), Subsurface storm flow formation at different hillslopes and implications for the 'old water paradox,' *Hydrol. Processes*, *22*, 104–116, doi:10.1002/hyp.6687.
Kirchner, J. W. (2006), Getting the right answers for the right reasons: Linking measurements, analyses, and models to advance the science of hydrology, *Water Resour. Res.*, *42*, W03S04, doi:10.1029/2005WR004362.
Kirchner, J. W., X. H. Feng, C. Neal, and A. J. Robson (2004), The fine structure of water-quality dynamics: The (high-frequency) wave of the future, *Hydrol. Processes*, *18*, 1353–1359, doi:10.1002/hyp.5537.
Klaus, J., E. Zehe, M. Elsner, C. Külls, and J. J. McDonnell (2013), Macropore flow of old water revisited: Experimental insights from a tile-drained hillslope, *Hydrol. Earth Syst. Sci.*, *17*(1), 103–118, doi:10.5194/hess-17-103-2013.
Klotz, D., and K. P. Seiler (1980), Labor und Geländeversuche zur Ausbreitung konservativer Tracer in fluvioglazialen Kiesen von Oberbayern, *GSF-Ber. R250*, pp. 74–89, GSF, Munich, Germany.
Koch, J. C., S. A. Ewing, R. Striegl, and D. M. McKnight (2013), Rapid runoff via shallow throughflow and deeper preferential flow in a boreal catchment underlain by frozen silt (Alaska, USA), *Hydrogeol. J.*, *21*(1), 93–106, doi:10.1007/s10040-012-0934-3.
Köhne, J. M., B. P. Mohanty, and J. Šimůnek (2006), Inverse dual-permeability modeling of preferential water flow in a soil column and implications for field-scale solute transport, *Vadose Zone J.*, *5*, 59–76, doi:10.2136/vzj2005.0008.
Laine-Kaulio, H. (2011), Development and analysis of a dual-permeability model for subsurface stormflow and solute transport in a forested hillslope, Doctoral thesis, *Aalto Univ. Publ. Ser., Doct. Diss. 71/2011*, Aalto Print, Helsinki. [Available at http://lib.tkk.fi/Diss/2011/isbn9789526042459/isbn9789526042459.pdf.]
Laine-Kaulio, H., T. Karvonen, H. Koivusalo, A. Laurén, and S. Saastamoinen (2009), Determination of till hydraulic properties for modelling flow and solute transport in a forested hillslope, *Geophys. Res. Abstr.*, *11*, EGU2009–11662-2.
Laine-Kaulio, H., H. Koivusalo, A. S. Komarov, M. Lappalainen, S. Launiainen, and A. Laurén (2014), Extending the ROMUL model to simulate the dynamics of dissolved and sorbed C and N compounds in decomposing boreal mor, *Ecol. Modell.*, *272*, 277–292, doi:10.1016/j.ecolmodel.2013.09.026.
Larsbo, M., and N. J. Jarvis (2003), MACRO5.0: A model of water flow and solute transport in macroporous soil, Tech. Description, *Stud. in the Biogeophys. Environ. Emergo 2003:6*, SLU, Dep. of Soil Sci., Uppsala, Sweden.
Lepistö, A., P. Seuna, and L. Bengtsson (1994), The environmental tracer approach in storm runoff studies in forested catchments, in *FRIEND: Flow Regimes from International Experimental and Network Data, Proceedings of the Braunschweig Conference*, edited by P. Seuna et al., *IAHS Publ. 221*, pp. 369–379, IAHS Press, Wallingford, October 1993.
Lind, B. B., and L. Lundin (1990), Saturated hydraulic conductivity of Scandinavian tills, *Nord. Hydrol.*, *21*, 107–118.
McDonnell, J. J. (1990), A rationale for old water discharge through macropores in a steep, humid catchment, *Water Resour. Res.*, *26*(11), 2821–2832.
McDonnell, J. J., and K. Beven (2014), Debates: The future of hydrological sciences: A (common) path forward? A call to action aimed at understanding velocities, celerities and residence time distributions of the headwater hydrograph, *Water Resour. Res.*, *50*, 5342–5350, doi:10.1002/2013WR015141.
McDonnell, J. J., and T. Tanaka (2001), On the future of forest hydrology and biogeochemistry, *Hydrol. Processes*, *15*, 2053–2055, doi:10.1002/hyp.351.
Mikola, P. (1982), Application of vegetation science to forestry in Finland, in *Handbook of Vegetation Science*, edited by G. Jahn, Part 12, pp. 199–224, Dr. W. Junk, Hague, Netherlands.
Mosley, M. P. (1979), Streamflow generation in a forested watershed, New Zealand, *Water Resour. Res.*, *15*(4), 795–806.
Möttönen, V. (2000), Variation in the hydraulic properties of forest soil before and after felling, Licentiate's thesis, Fac. of For. Sci., Univ. of Joensuu, Joensuu, Finland.

Ogata, A., and R. B. Banks (1961), A solution of the differential equation of longitudinal dispersion in porous media, *U.S. Geol. Surv. Prof. Pap., 411-A*, 9 pp.
Pearce, A. J., M. K. Stewart, and M. G. Sklash (1986), Storm runoff generation in humid headwater catchments. 1: Where does the water come from?, *Water Resour. Res.*, *22*(8), 1263–1272.
Pickens, F. J., and E. G. Grisak (1980), Scale-dependent dispersion in a stratified granular aquifer, *Water Resour. Res.*, *17*(4), 1191–1211.
Piirainen, S., L. Finér, H. Mannerkoski, and M. Starr (2007), Carbon, nitrogen and phosphorus leaching after site preparation at a boreal forest clear-cut area, *For. Ecol. Manage.*, *243*, 10–18, doi:10.1016/j.foreco.2007.01.053.
Rausch, R., W. Schäfer, R. Therrien, and C. Wagner (2005), *Solute Transport Modelling. An Introduction to Models and Solution Strategies*, Gebr. Bornträger Verlagsbuchhandlung, Stuttgart, Germany.
Ray, C., T. R. Ellsworth, A. J. Valocchi, and C. W. Boast (1997), An improved dual porosity model for chemical transport in macroporous soils, *J. Hydrol.*, *193*, 270–292.
Ray, C., T. Vogel, and J. Dušek (2004), Modeling depth-variant and domain-specific sorption and biodegradation in dual-permeability media, *J. Contam. Hydrol.*, *70*, 63–87, doi:10.1016/j.jconhyd.2003.08.009.
Richards, L. A. (1931), Capillary conduction of liquids through porous medium, *Physics*, *1*(5), 318–333.
Seibert, J. (1999), Conceptual runoff models—Fiction or representation of reality?, Doctoral dissertation, Acta Univ. Ups., *Comprehensive Summaries of Uppsala Dissertations from the Faculty of Science and Technology*, vol. 436, Uppsala Univ., Uppsala, Sweden.
Sidle, R. C., S. Noguchi, Y. Tsuboyama, and K. Laursen (2001), A conceptual model of preferential flow systems in forested hillslopes: Evidence of self-organization, *Hydrol. Processes*, *15*, 1675–1692.
Šimůnek, J., M. Šejna, and M. Th. van Genuchten (1999), *The HYDRUS-2D Software Package for Simulating Two-Dimensional Movement of Water, Heat, and Multiple Solutes in Variably Saturated Media*, Version 2.0, *IGWMC-TPS-53*, Int. Ground Water Model. Center, Colorado Sch. of Mines, Golden, Colo.
Šimůnek, J., N. J. Jarvis, M. Th. van Genuchten, and A. Gärdenäs (2003), Review and comparison of models for describing non-equilibrium and preferential flow and transport in the vadose zone, *J. Hydrol.*, *272*, 14–35.
Šimůnek, J., M. Šejna, and M. Th. van Genuchten (2012), *The DualPerm Module for HYDRUS (2D/3D). Simulating Two-Dimensional Water Movement and Solute Transport in Dual-Permeability Variably-Saturated Porous Media*, Version 1, Dep. of Environ. Sci. Univ. of California Riverside, Riverside, Calif., and PC Progress Ltd., Prague.
Spitz, K., and J. Moreno (1996), *A Practical Guide to Groundwater and Solute Transport Modeling*, John Wiley, N. Y.
Tracy, F. T. (1995), l-D, 2-D, and 3-D analytical solutions of unsaturated flow in groundwater, *J. Hydrol.*, *170*, 199–214.
Uchida, T., I. Tromp-van Meerveld, and J. J. McDonnell (2005), The role of lateral pipe flow in hillslope runoff response: An intercomparison of nonlinear hillslope response, *J. Hydrol.*, *311*, 117–133, doi:10.1016/j.jhydrol.2005.01.012.
Vaché, K., and J. J. McDonnell (2006), A process-based rejectionist framework for evaluating catchment runoff model structure, *Water Resour. Res.*, *42*, W02409, doi:10.1029/2005WR004247.
Vakkilainen, P. (1982), On the estimation of evapotranspiration, Doctoral thesis [in Finnish], Acta Universitatis Ouluensis C 20, Artes Construction 6, Univ. of Oulu, Oulu, Finland.
van Genuchten, M. Th. (1980), A closed-form equation for predicting the hydraulic conductivity of unsaturated soils, *Soil Sci. Soc. Am. J.*, *44*, 892–898.
van Genuchten, M. Th., and W. G. Gray (1978), Analysis of some dispersion corrected numerical schemes for solution of the transport equation, *Int. J. Numer. Methods Eng.*, *12*, 387–404.
Vogel, T., H. H. Gerke, R. Zhang, and M. Th. van Genuchten (2000), Modeling flow and transport in a two-dimensional dual-permeability system with spatially variable hydraulic properties, *J. Hydrol.*, *238*, 78–89.
Vogel, T., L. Lichner, J. Dušek, and A. Čipáková (2007), Dual-continuum analysis of a cadmium tracer field experiment, *J. Contam. Hydrol.*, *92*, 50–65, doi:10.1016/j.jconhyd.2007.01.001.
Wang, H. F., and M. P. Anderson (1982), *Introduction to Groundwater Modeling. Finite Difference and Finite Element Methods*, W. H. Freeman, San Francisco, Calif.
Warsta, L. (2011), Modelling water flow and soil erosion in clayey, subsurface drained agricultural fields, Doctoral thesis, *Aalto Univ. Publ. Ser., Doct. Diss. 82/2011*, Aalto Print, Helsinki. [Available at http://lib.tkk.fi/Diss/2011/isbn9789526042893/isbn9789526042893.pdf.]
Warsta, L., T. Karvonen, H. Koivusalo, M. Paasonen-Kivekäs, and A. Taskinen (2013), Simulation of water balance in a clayey, subsurface drained agricultural field with three-dimensional FLUSH model, *J. Hydrol.*, *476*, 395–409, doi:10.1016/j.jhydrol.2012.10.053.
Weiler, M., and F. Naef (2000), Verification of flow processes in soils with combined sprinkling and dye tracer experiments, in *Proceedings of the International Workshop on Runoff Generation and Implications for River Basin Modelling*, edited by C. Leibundgut et al., pp. 345–355, IAHS, Freiburg, Germany.
Weiler, M., and F. Naef (2003), Simulating surface and subsurface initiation of macropore flow, *J. Hydrol.*, *273*(1), 139–154.
Weiler, M., and J. J. McDonnell (2007), Conceptualizing lateral preferential flow and flow networks and simulating the effects on gauged and ungauged hillslopes, *Water Resour. Res.*, *43*, W03403, doi:10.1029/2006WR004867.